doi: 10.3969/j.issn.1673-9736.2017.02.07
**Article ID:** 1673-9736(2017)02-0118-13

# Cumulative gain and lift charts for model performance assessment in mineral potential mapping

WU Wei[1] and CHEN Yongliang[2*]

1. *Changchun Institute of Urban Planning and Design, Changchun 130033, China;*
2. *Institute of Mineral Resources Prognosis on Synthetic Information, Jilin University, Changchun 130026, China*

**Abstract:** Model performance assessment is a key procedure for mineral potential mapping, but the corresponding research achievements are seldom reported in literature. Cumulative gain and lift charts are well known in the data mining community specialized in marketing and sales applications and widely used in customer churn prediction for model performance assessment. In this paper, they are introduced into the field of mineral potential mapping for model performance assessment. These two charts can be viewed as a graphic representation of the advantage of using a predictive model to choose mineral targets. A cumulative gain curve can represent how much a predictive model is superior to a random guess in mineral target prediction. A lift chart can express how much more likely the mineral targets predicted by a model are deposit-bearing ones than those by a random selection. As an illustration, the cumulative gain and lift charts are applied to measure the performance of weights of evidence, logistic regression, restricted Boltzmann machine, and multilayer perceptron in mineral potential mapping in the Altay district in northern Xinjiang in China. The results show that the cumulative gain and lift charts can visually reveal that the first three models perform well while the last one performs poorly. Thus, the cumulative gain and lift charts can serve as a graphic tool for model performance assessment in mineral potential mapping.

**Key words:** cumulative gain and lift charts; mineral potential mapping performance assessment; weights of evidence; logistic regression; restricted boltzmann machine; multilayer perceptron

## 1 Introduction

Mineral potential mapping is a key step to distinguish mineral targets in an area of interest in mineral exploration. A variety of approaches have been reported in the literature, such as weights of evidence or WofE (Agterberg, 1990, 1992; Agterberg *et al.*, 1990; Bonham-Carter *et al.*, 1988, 1989; Carranza & Hale, 2002a; Nykänen *et al.*, 2008; Tangestani & Moore, 2001; Xu *et al.*, 1992), logistic regression or LGR (Agterberg, 1974, 1989; Agterberg and Bonham-Carter, 1999; Carranza & Hale, 2001; Chen *et al.*, 2011; Nykänen *et al.*, 2008), restricted Boltzmann machines or RBM (Chen, 2014), and multilayer perceptron or MLP (Skabar, 2007), to name only a few. However, the techniques for assessing the performance of mineral potential mapping models are seldom reported in the literature. Model performance assessment is a measure of accuracy of mineral potential mapping results. It provides a feasible way to

Received 5 December 2015, accepted 20 December 2015
* Corresponding author (chenyongliang2009@hotmail.com)
Supported by Project of the National Natural Science Foundation of China (Nos. 41272360, 41472299, 61133011).

compare the effectiveness of different mineral potential mapping models. Thus, it is necessary to set up common techniques to assess the performance of mineral potential mapping models in mineral exploration.

Cumulative gain and lift charts are well known in the data mining community specialized in marketing and sales applications (Berry & Linoff, 1999) and widely used in customer churn prediction for model performance assessment (Anjum, 2014; Piatetsky-Shapiro and Steingold, 2000; Verbeke *et al.*, 2011; Xie *et al.*, 2009). The class imbalance data used in customer churn prediction (Burez & Van den Poel, 2009; Japkowicz, 2000) are quite similar to the multivariate data used in mineral potential mapping. Therefore, the cumulative gain and lift charts are introduced into the field of mineral potential mapping for model performance assessment. For demonstration purpose, the cumulative gain and lift charts are applied to evaluate the performance of WofE, LGR, RBM, and MLP models in mineral potential mapping in the Altay district in northern Xinjiang in China. The result illustrates that the cumulative gain and lift charts can serve as a graphic tool for the model performance assessment in mineral potential mapping. The theory of cumulative gain and lift charts is introduced in Section 2 and the method based on the cumulative gain and lift charts for the performance assessment of mineral potential mapping models is discussed in Section 3. A case study follows in Section 4 and finally the conclusion.

## 2 Cumulative gain and lift charts

In dealing with a binary classification problem, one class can be always labeled as a positive and the other one as a negative class. Assume that the test set consists of $p$ positive and $n$ negative examples. A classifier assigns a class label to each of them, but some of the assignments are wrong. To assess the classification results, the number of true positive ($tp$), true negative ($tn$), false positive ($fp$) (actually negative, but classified as positive) and false negative ($fn$) (actually positive, but classified as negative) examples can be counted. They satisfy

$$tp + fn = p; tn + fp = n \tag{1}$$

The classifier assigned $tp + fp$ examples to the positive class and $tn + fn$ examples to the negative class. The following measures can be defined:

$$\text{fprate} = 1 - \text{specificity} = \frac{fn}{n} \tag{2}$$

$$\text{tprate} = \text{sensitivity} = \frac{tp}{p} \tag{3}$$

$$\text{yrate} = \frac{tp + fp}{p + n} \tag{4}$$

$$\text{lift} = \frac{\text{tprate}}{\text{yrate}} = \frac{\text{sensitivity}}{(tp + fp)/(p + n)} \tag{5}$$

The fprate measures the fraction of negative examples that are misclassified as positive ones. The tprate or sensitivity measures the fraction of positive examples correctly classified. The yrate measures the fraction of examples that are classified as positive ones. The lift is a measure of the effectiveness of a model calculated as the ratio between the results obtained with and without the model.

A classification model is a function that $f: X \to [0,1]$ maps each example $x$ to a real number $f(x)$. Usually, a threshold $t$ is chosen for which the examples where $f(x) \geq t$ are considered positive examples and the others are considered negative examples. This implies that each pair of a classifier and threshold $t$ defines a binary classifier. Thus, a binary classifier system can be obtained by varying threshold $t$.

A cumulative gain curve is a graphical plot which illustrates performance of the binary classifier system as its discrimination threshold $t$ is varied. It is created by plotting the sensitivity against the yrate at various threshold settings.

In a cumulative gain curve, each binary classifier for a given test set of examples is represented by a point (yrate, tprate). By varying the threshold of the classifier, a set of binary classifiers represented with a set of points on the chart are obtained. It gives a graphic interpretation of what percentage of examples one has to target to reach a certain percentage of all positive examples. A purely random model is presented by a point on the baseline through (0, 0) and (100%, 100%) (Fig. 1).

The position and shape of a cumulative gain curve depend on the classification result and the percentage of positive examples in a test set. In the yrate-tprate space, if the classification is perfect (one-hundred percent of test examples are correctly classified), the cumulative gain curve is located near to the tope left corner (Fig. 1); and the lower the percentage of positive examples is, the nearer to the tope left corner the cumulative gain curve of the perfect classification is located (Fig. 1b).

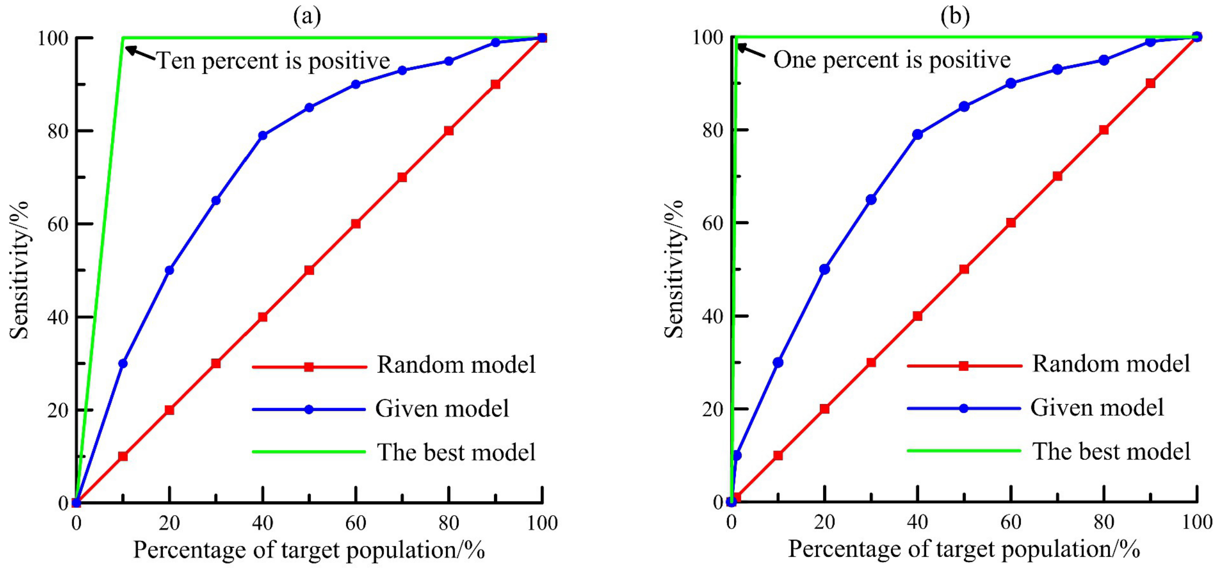


**ig. 1 Cumulative gain curves for a test set of examples with (a) ten percent positives and (b) one percent positives**

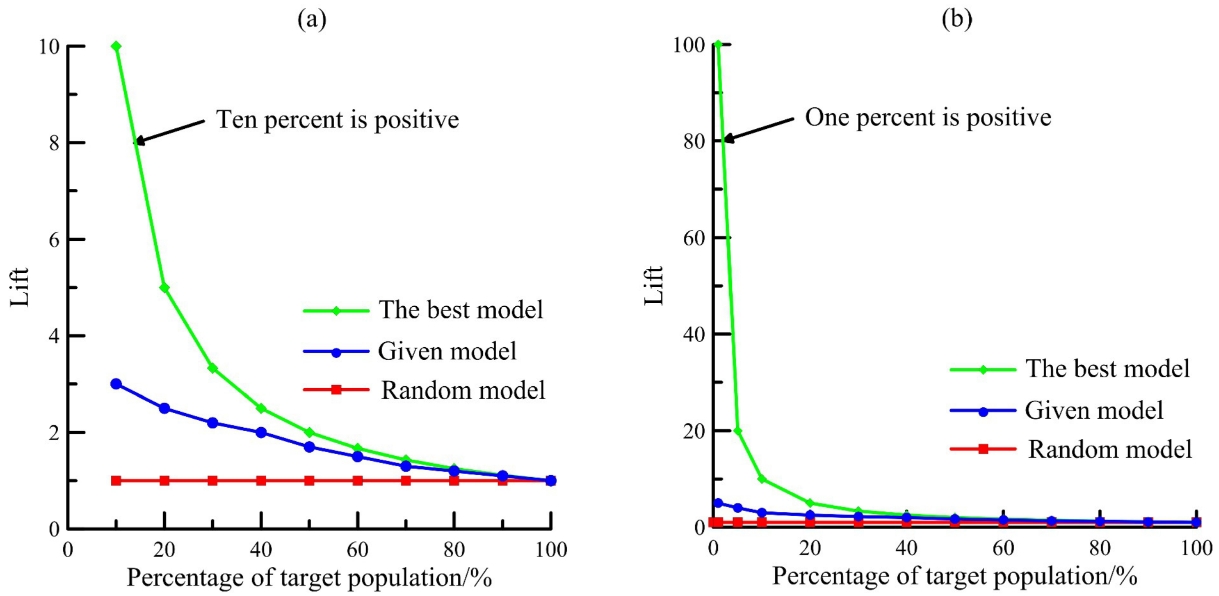


**Fig. 2 Cumulative lift charts for a test set of examples with (a) ten percent positives and (b) one percent positives**

A cumulative lift chart is derived from the corresponding cumulative gain curve. Its horizontal coordinate is the same as that of the cumulative gain chart and its vertical coordinate is the ratio of vertical coordinate, compared to horizontal coordinate of the cumulative gain curve.

In a cumulative lift chart (Fig. 2), a point (yrate, tprate/yrate) is used to express a binary classifier for a given test set of examples. Thus, a set of points representing a set of binary classifiers with respect to varying thresholds form the cumulative lift curve that tells how much better a binary classifier predicts compared to the random selection by comparing the sensitivity to the overall positive rate in the test set. A purely random selection is presented by a point on the baseline through ($pp$, 1) and (100%, 1), here $pp$ denotes the percentage of positive examples in a test set. As the derived chart of a cumulative gain curve, the shape of a lift curve is also affected by the percentage of positive examples. When the percentage of positive examples becomes smaller, the lift curve will become nearer to horizontal and vertical axes as well as the origin (Fig. 2b).

The performance of different models can be differentiated by drawing their cumulative gain and lift charts. It is intuitive that the greater the separation between the cumulative gain or lift curve and the baseline, the better the model performs. If one model has separation across the entire ranking greater than another model with the same definition of the target variable, then the dominate model wins.

However, it may not be the case that one model is strictly dominating over the other in practical situations. It is easy to imagine that the gain curves of different models may cross. In this situation, the area under the cumulative gain curve or $AUL$ (Bekkar *et al.*, 2013) can be applied to measure the overall performance of different models. Based on the definition given by Tuffery (2005), the $AUL$ can be written as

$$AUL = \frac{p}{2(p+n)} + \left(1 - \frac{p}{p+n}\right) \times AUC \quad (6)$$

where: $p$ and $n$ are the number of positive and negative examples, respectively; and $AUC$ is the area under the ROC curve (the receiver operating characteristic curve) (Flach *et al.*, 2011). The $AUC$ value can be estimated by the Wilcoxon Mann-Whitney test (Bergmann *et al.*, 2000). Let $x_i$ ($i = 1, 2, \cdots, p$) represent the predicted value of the $i$th positive example and $y_j$ ($j = 1, 2, \cdots, n$) represent the predicted value of the $j$th negative example. Then, the $AUC$ value can be estimated by

$$AUC = \frac{1}{pn} \sum_{i=1}^{p} \sum_{j=1}^{n} \varphi(x_i, y_j) \quad (7)$$

$$\varphi(x_i, y_i) = \begin{cases} 1, & x_i > y_j \\ 0.5, & x_i = y_j \\ 0, & x_i < y_j \end{cases} \quad (8)$$

If the classification performance is perfect, the $AUC$ value is 1 with respect to that the $AUL$ value equals $(2n+p)/(2n+2p)$; if the classification performance is equivalent to a complete random guess, both the $AUC$ and $AUL$ values are 0.5. Usually, an $AUC$ value falls somewhere between 0.5 and 1 with respect to that the corresponding $AUL$ value is in the interval $[0.5, (2n+p)/(2n+2p)]$. If $p/(p+n)$ is very small, the areas under the two curves are very close. In all cases, to deduce that a model is superior to another, it is equivalent to measuring their $AUC$s or $AUL$s, i.e., if $AUC1 > AUC2$ or $AUL1 > AUL2$.

# 3 Mineral potential mapping performance assessment

Deposit-bearing phenomenon in mineral exploration is similar to customer churn in service industry. Customer churn is a rare event in service industries, but of great interest and great value. Similarly, deposit-bearing is also a rare event in mineral exploration, but of great interest and great value.

In customer churn prediction, a predictive model assigns a score to each of customer examples and then a discrimination threshold is used to classify the customer examples into churners and non-churners. The number of true churners, true non-churners, false churners and false non-churners can be counted and used to calculate the measures of yrate, tprate, and lift. As the discrimination threshold is varied, the measures of yrates, tprates, and lifts at various threshold settings can be obtained and used to draw cumulative gain and lift charts.

In mineral exploration, suppose that the area of interest has been divided into a set of grid cells. Then deposit-bearing and non-deposit-bearing cells can be identified by superimposing the map of known mineral deposits over the map of grid cells. The deposit-bearing cells denote those cells in which a known mineral deposit has been found while non-deposit-bearing cells are those cells in which no known mineral deposits has been found. The deposit-bearing and non-deposit-bearing cells in mineral exploration can be viewed as the counterparts of churners and non-churners in service industries.

In mineral potential mapping, a statistical model is used to predict deposit-bearing favorability of each cell and a threshold is used to separate mineral target cells from the grid cell population. The mineral target and non-mineral target cells are the predicted deposit-bearing and non-deposit bearing cells, respectively. Referring to the method of model performance assessment in customer churn prediction, the number of true deposit-bearing, true non-deposit-bearing, false deposit-bearing, and false non-deposit-bearing cells can be counted and used to compute the measures of yrate, tprate, and lift. By varying the threshold, the measures of yrates, tprates, and lifts at various threshold settings can be obtained and used to draw cumulative gain and lift charts.

Choosing a set of threshold values is the key step for drawing the cumulative gain and lift charts in mineral potential mapping. It is reasonable to suppose that $k$ thresholds evenly distributed between the minimum and maximum values of the deposit-bearing favorability predicted by the model. Then the increment between two neighboring thresholds can be determined by

$$\Delta = (f\max - f\min)/k, \tag{9}$$

where $fmax$ and $fmin$ are the maximum and minimum values of the deposit-bearing favorability predicted by the model. These two values can serve as the first and last thresholds, respectively. Then the $j$ th ($j = 1, 2, \cdots, k$) threshold can be computed by

$$f_j = f\min + \Delta^* (k - j) \tag{10}$$

The cumulative gain and lift charts can graphically interpret the performance of a mineral potential mapping model. The farther the cumulative gain and lift charts of a model are away from the baseline, the better the model performs. In practice, *AUL*s can be computed as an overall performance measure in case different models have quite similar cumulative gain and lift charts. The larger the *AUL* of a model, the better the model performs.

## 4 Case study

The Altay district in northern Xinjiang in China is chosen as the study area. The WofE, LGR, RBM, and MLP are applied to the mineral potential mapping and their performance is assessed using cumulative gain and lift charts.

### 4.1 Geological setting and mineral deposits

The study area is located in the Altay orogenic belt, which is the amalgamated part of the Siberia plate and the Kazakhstan-Junggar plate (Li, 1996; Li & Zhao, 2002). During Devonian and Early Carboniferous periods, the south continental margin of the Siberia plate became an active continental margin and formed the geotectonic environment of gutter (Wulungu trench)-arc (Kalatongke island arc)-basin (crane back arc basin) system due to the subduction of the Junggar plate (Li, 1996; Li & Zhao, 2002). In the process of the Junggar plate subduction, the collision and amalgamation of the Siberia, Khazakstan, and Junggar blocks resulted in the evolution of geotectonic environment that provided good congenital, parturient and postnatal conditions for polymetallic mineralization (Zeng *et al.*, 2005). The Ashele large-sized copper-zinc deposit, the Duolanasayi large-sized gold deposit, and two dozens of other mineral deposits have been found in the area. Fig. 3 shows the simplified geologic map with the known mineral deposits and geochemical sample locations.

The mineralization of copper, gold, and other metallogenic elements in the study area was closely related to the Altay orogenic process (Li, 1996; Li & Zhao, 2002). The Ashele copper-zinc deposit was formed in the Ashele volcanic-sedimentary basin in the foreland during the orogenic intermittent extensional period; and the Duolanasayi gold deposit was formed in the southern margin of the Altay orogenic belt during the main orogenic period. The volcanic-magmatic activities, volcanic sedimentation, tectonic-magmatic activities, and hydrothermal activities in the Altay orogenic belt are the essential controlling factors for all the types of mineralization.

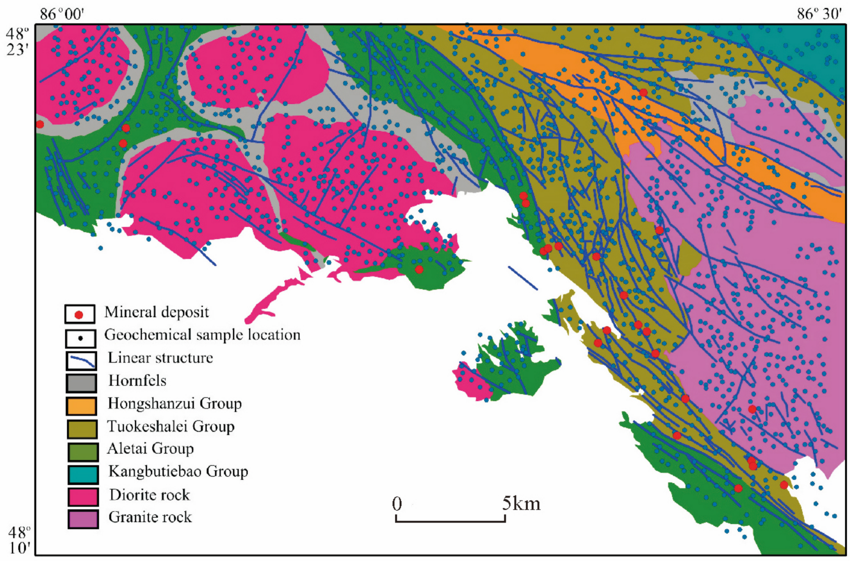


**Fig. 3 Simplified geologic map with the known mineral deposits and geochemical sample locations**

## 4.2 Geological map patterns

Based on the discussions in Section 4.1, it can be concluded that the tectonic movements, volcanic-sedimentary activities, magmatic intrusions, and hydrothermal activities were genetically related to the polymetallic mineralization. Consequently, linear structures, the early-middle Devonian and early Carboniferous systems, acidic-neutral magmatic rocks, and hornfels zones are chosen as geological map patterns.

The likelihood ratios or *LR*s (Chen, 2014) were applied to determine the optimal buffering width of linear structures. The *LR* is a measure of the spatial relationship between a map pattern and the known mineral deposits in a study area. Suppose that the study area has been divided into a set of grid cells. Let *AR* and *DR* denote the fraction of the grid cells within the buffered linear structures and the fraction of the known mineral deposits within the buffered linear structures, respectively. Then, *LR* is defined as

$$LR = DR/AR \tag{11}$$

The values of *LR*s are within interval $[0, \infty)$. If $0 \leq LRs \leq 1.0$, the buffered linear structures are approximately equal to the areas chosen by a random guess; and if $LRs > 1.0$, the buffered linear structures are better than the areas chosen by a random guess. According to Eq. (11), a large *LR* means that the buffered linear structures are only a small fraction of the study area but bear a large fraction of the known mineral deposits.

In our case study, the area is divided into 100 × 151 grid cells. Except for 6 852 cells located in the blank area, the other 8 248 cells (8 223 non-deposit-bearing and 25 deposit-bearing cells) were used to compute the *LR*s of the linear structures buffered different widths. Each buffering width corresponds to one value of *LR*s and the optimal one is with respect to the maximum value of *LR*s. The optimal buffering width was selected from the following predefined buffering widths: 0.01 km, 0.05 km, 0.075 km, 0.1 km, 0.2 km, 0.3 km, 0.4 km, and 0.5 km. Fig. 4 shows that the *LR* reaches its maximum value at 0.075 km. Thus, 0.075 km was the optimal buffering width. After being buffered, intersections of some of the linear structures become apparent. The intersections of the buffered linear structures serve as a derivative geological map pattern.

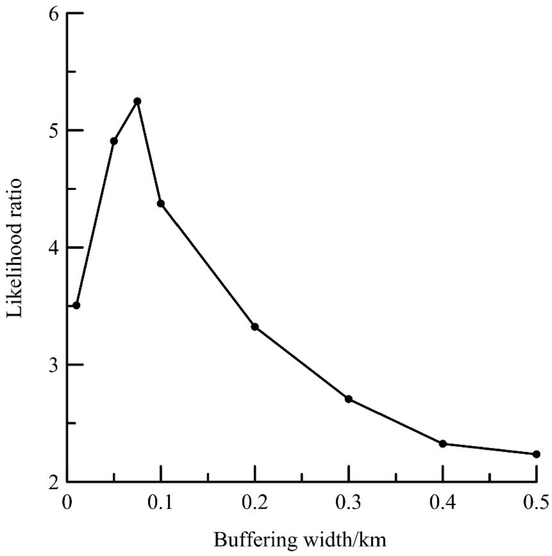


**Fig. 4 Diagram of *LR*s varying with buffering widths**

## 4.3 Geochemical map patterns

Au, Ag, Cu, Pb, and Zn serve as the geochemical indicative elements and the grid data of these five elements, which match with the grid cells used in Section 4.2, are generated using the Golden Software Surfer.

The *LR* is applied to choose the optimal threshold for identifying geochemical anomalies. For each element, 1 000 thresholds were predefined to distribute uniformly between the minimum and maximum concentration values of the element. The *LR*, with respect to each threshold, is computed and the threshold with respect to the maximized *LR* is chosen as the optimal threshold. Table 1 lists the maximized *LR*s with respect to the optimal thresholds for the five elements. The delineated geochemical anomalies then serve as geochemical map patterns.

**Table 1 *LR*s with respect to the optimal thresholds for the five geochemical elements**

| | Au | Ag | Cu | Pb | Zn |
|---|---|---|---|---|---|
| Maximized *LR*s | 57.217 | 36.411 | 20.026 | 57.217 | 400.520 |
| Optimal thresholds | 99.553 | 0.874 | 360.260 | 89.954 | 411.931 |

## 4.4 Map pattern selection

The 8248 cells were used to estimate *LR* of each map pattern. The estimated *LR*s for all the map patterns are listed in Table 2. A map pattern with *LR* more than one can be selected as a significant map pattern for mineral potential mapping. From Table 2, it can be seen that there are nine map patterns with *LR*s more than one. They are as follows: (a) gold geochemical anomaly, (b) silver geochemical anomaly, (c) copper geochemical anomaly, (d) lead geochemical anomaly, (e) zinc geochemical anomaly, (f) the buffered linear structures, (g) the middle Devonian Tuokesalei Group, (h) the middle Devonian Aletai Group, and (i) the intersections of buffered linear structures.

**Table 2 *LR*s for the 14 binary map patterns**

| Map pattern | *LR*s | Map pattern | *LR*s |
|---|---|---|---|
| Gold geochemical anomaly | 86.143 | Acidic magmatic rock | 0.677 |
| Silver geochemical anomaly | 54.818 | Neutral magmatic rock | 0.0 |
| Copper geochemical anomaly | 30.150 | The Tuokesalei Group | 2.808 |
| Lead geochemical anomaly | 86.143 | The Aletai Group | 4.746 |
| Zinc geochemical anomaly | 603.0 | The Kangbutiebao Group | 0.0 |
| Hornfels zone | 0.854 | The Hongshanzui Group | 0.0 |
| Linear structure | 5.248 | Intersection of linear structures | 9.726 |

## 4.5 The WofE modeling

The contingency table test (Agterberg and

Cheng, 2002) for the nine pairwise map patterns are implemented and the results are listed in Table 3. It can be seen that the 9 map patterns basically satisfy pairwise conditional independent assumption.

**Table 3 Pairwise Chi-squared tests for the 9 selected map patterns**

| | (b) | (c) | (d) | (e) | (f) | (g) | (h) | (i) |
|---|---|---|---|---|---|---|---|---|
| (a) | 0.3906 | 0.3906 | 0.3906 | 0.3906 | 0.0271 | 1.1905 | 0.2500 | 0.3906 |
| (b) | | 0.3906 | 5.9920 | 5.9920 | 0.1082 | 0.8267 | 0.1111 | 0.3906 |
| (c) | | | 0.3906 | 0.3906 | 0.0271 | 0.8267 | 0.1111 | 0.3906 |
| (d) | | | | 5.9920 | 0.1082 | 0.8267 | 0.1111 | 0.3906 |
| (e) | | | | | 0.1082 | 0.8267 | 0.1111 | 0.3906 |
| (f) | | | | | | 6.3131 | 2.9264 | 0.1082 |
| (g) | | | | | | | 13.7620 | 0.8267 |
| (h) | | | | | | | | 0.1111 |

Note: The numbers from (*a*) through (*i*) are the code numbers of nine selected binary map patterns.

For each map pattern, two weights and their variances and the variance due to missing data are estimated and listed in Table 4. The posterior probability and posterior probability deviation maps are shown in Fig. 5. The new conditional independence test (Agterberg & Cheng, 2002) is applied to test overall conditional independence, the estimated $T = 30.238$. The 95% confidence limit is $1.645 \times 6.644 = 10.929$ for $T-n = 30.238-25 = 5.238$. Thus the conditional independence hypothesis should be accepted.

**Table 4 Weights, weight variances, and the variances due to missing data of the 9 selected map patterns**

| Map patterns | $W^+$ | $(W^+)$ | $W^-$ | $(W^-)$ | (missing) |
|---|---|---|---|---|---|
| Gold geochemical anomaly | 3.850 | 1.143 | −0.0400 | 0.0418 | 1.444e−05 |
| Silver geochemical anomaly | 3.398 | 1.091 | −0.0395 | 0.0418 | 9.396e−06 |
| Copper geochemical anomaly | 2.800 | 1.050 | −0.0384 | 0.0418 | 5.075e−06 |
| Lead geochemical anomaly | 3.850 | 1.143 | −0.0400 | 0.0418 | 1.444e−05 |
| Zinc geochemical anomaly | 5.796 | 2.000 | −0.0407 | 0.0418 | 5.990e−05 |
| Linear structure | 1.052 | 0.0917 | −0.4130 | 0.0716 | 5.727e−06 |
| The Tuokesalei Group | 0.427 | 0.1440 | −0.1270 | 0.0557 | 5.771e−07 |
| The Aletai Group | 0.951 | 0.0672 | −0.653 | 0.1000 | 6.930e−06 |
| Intersection of linear structures | 1.669 | 1.016 | −0.0333 | 0.0418 | 1.270e−06 |

## 4.6 LGR modeling

In LGR model, deposit-bearing probability is expressed as a function of map patterns. The optimized regression coefficients can be sought using conjugate gradient (CG) optimization of a log-linear model. Usually, this algorithm can obtain a group of nearly optimized regression coefficients after 20 times of iterations.

The 8 248 cells were used to establish a LGR model. The CG algorithm was used to seek the optimized regression coefficients. After 50 times of iterations, the optimized regression coefficients were obtained (Table 5). The deposit-bearing probability map is shown in Fig. 6.

## 4.7 RBM modeling

In mineral potential mapping, a RBM can be

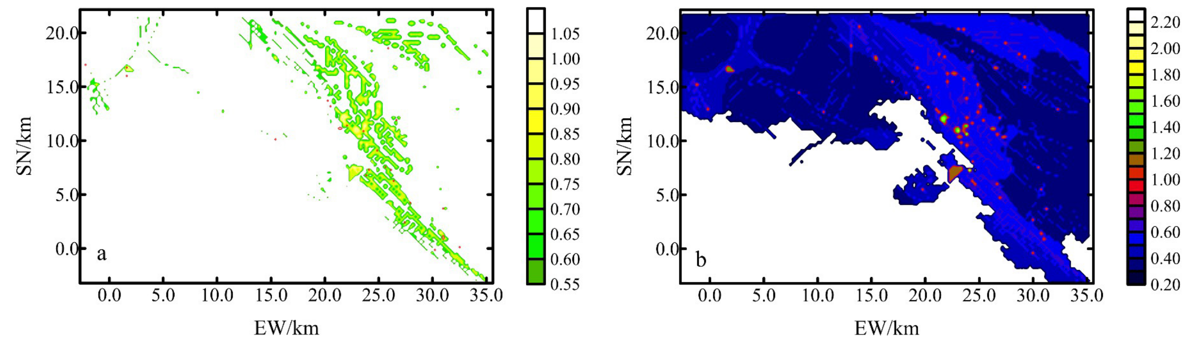


**Fig. 5 Posterior probability map (a) and posterior probability deviation map (b)**

**Table 5 Estimated constant and regression coefficients**

| Map patterns | Regression coefficients |
|---|---|
| Constants | -3.763 |
| Gold geochemical anomaly | 1.319 |
| Silver geochemical anomaly | 0.506 |
| Copper geochemical anomaly | 1.027 |
| Lead geochemical anomaly | 0.578 |
| Zinc geochemical anomaly | 0.951 |
| Linear structure | 0.484 |
| The Tuokesalei Group | 0.934 |
| The Aletai Group | 1.096 |
| Intersection of linear structures | 0.169 |

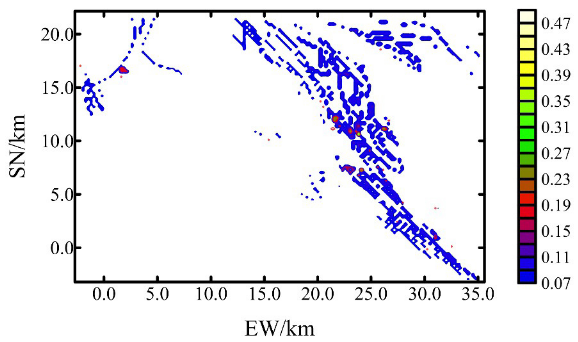


**Fig. 6 Deposit-bearing probability maps after 50 iterations**

trained for capturing the general features of the training cells. Based on a trained RBM, average square contribution or *ASC* and average square error or *ASE* can be computed and their thresholds can be defined (Chen, 2014). The training cells with the values of *ASC* or *ASE* more than the threshold are recognized as mineral targets. In practice, it is difficult to determine whether a training RBM is really converged. Empirically, a RBM can become approximately converged after more than 100 iterative training.

A RBM with 10 visible units representing the nine map patterns and 37 hidden units was constructed and applied to mineral potential mapping in the study area. The following parameters were empirically chosen: (a) learning rates; (b) weight cost = 0.000 2; and (c) learning moment = 0.9. The model is trained on the 8 248 cells for 200 epochs. After the training, the two mineral potential maps, with respect to *ASC*s and *ASE*s, are obtained (Fig. 7).

### 4.8 MLP modeling

A MLP is a feed forward network that maps an input vector onto an appropriate target vector. It uses a supervised back propagation training technique. In mineral potential mapping, a MLP can serve as a soft binary classifier to separate deposit-bearing and non-deposit-bearing cells.

A three-layer perceptron network is constructed for predicting mineral targets in the study area. The input layer, hidden layer, and output layer have, respectively, 9, 18, and 1 units. The sigmoidal function serve as the activation function and values of 0.000 5 and 0.9 serve as learning rate and momentum, respectively. The maximum training time was empirically defined as 200. The mineral potential map is obtained from the classification scores generated by the tvained model (Fig. 8).

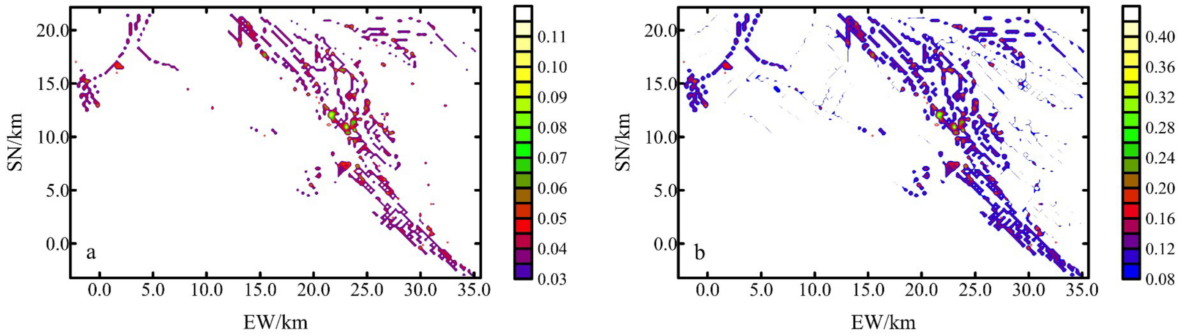


**Fig. 7 Mineral potential maps of *ASC*s (a) and *ASE*s (b) at epoch 200**

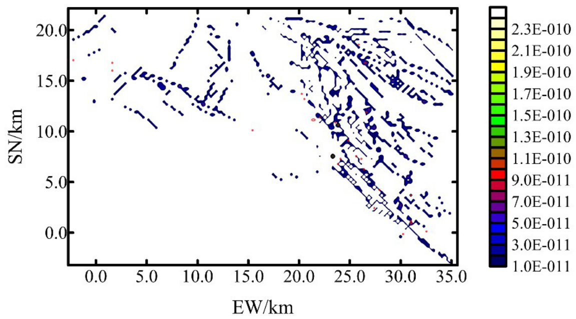


**Fig. 8 Mineral potential maps based on MLP classification scores at epoch 200**

## 4.9 Performance assessment

The cumulative gain and lift charts are applied to assess the effectiveness of the five mineral potential maps drawn in Sections 4.5 through 4.8. The threshold-defining method in Section 3 is used to predefine 1 000 thresholds for each mineral potential map, the yrate, tprate, and lift with respect to each threshold are estimated and the cumulative gains and lift charts are drawn in Fig. 9. The *AUC*, *AUL*, $SE_{\mathrm{AUC}}$, and $Z_{\mathrm{AUC}}$ with respect to each mineral potential map are computed and listed in Table 6.

The cumulative gain curves in Fig. 9a illustrate: (a) LGR performs a little bit better than WofE; (b) *ASC* and *ASE* perform same well due to the overlap of the two curves; (c) MLP performs worst among the five methods; and (d) the performance of both *ASC* and *ASE* are unable to be differentiated from that of LGR or WofE due to their crossed cumulative gain curves.

The cumulative lift charts in Fig. 9b show that: (a) the cumulative lift charts for LGR, *ASC*, and *ASE* have almost same shape and the maximum lift points locate far away from the origin; (b) the cumulative lift chart of WofE is similar to that of the above three methods, but the maximum lift points locate much nearer to the origin; and (c) MLP model has a cumulative lift chart near to the baseline and the maximum lift points locate around the origin.

According to the above features of the cumulative lift charts, we can conclude that: (a) LGR, *ASC*, and *ASE* perform best; (b) WofE performs well but a little bit worse compared to LGR, *ASC*, and *ASE*; (c) MLP performs worst among the five methods; and (d) LGR, *ASC*, and *ASE* can predict more concentrated mineral potential areas than WofE.

**Table 6 Overall performance measures of 5 mineral potential maps**

| Model | Epoch | Result | *AUC* | *AUL* | $SE_{\mathrm{AUC}}$ | $Z_{\mathrm{AUC}}$ |
|---|---|---|---|---|---|---|
| WofE | – | Posterior probability | 0.802 2 | 0.801 3 | 0.053 2 | 5.681 7 |
| LGR | 50 | Probability | 0.806 6 | 0.805 7 | 0.052 8 | 5.806 1 |
| RBM | 200 | *ASC* | 0.805 7 | 0.804 8 | 0.052 9 | 5.781 2 |
| RBM | 200 | *ASE* | 0.805 7 | 0.804 8 | 0.052 9 | 5.781 2 |
| MLP | 200 | Score | 0.658 0 | 0.657 5 | 0.059 8 | 2.640 6 |

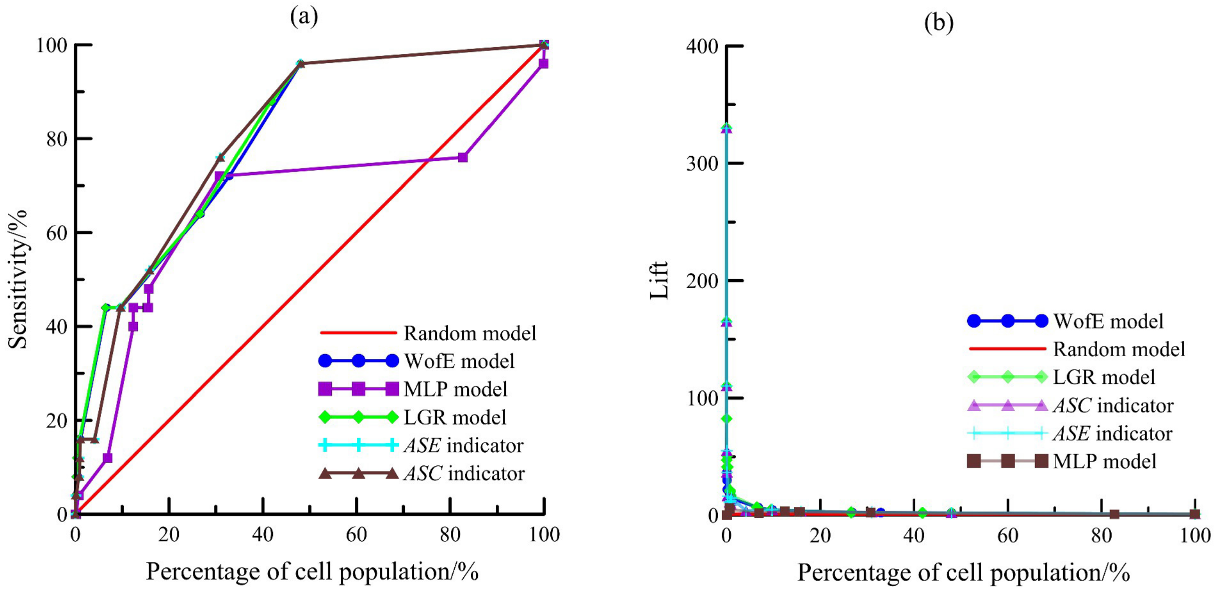


**Fig. 9 Cumulative gains (a) and lift charts (b) with respect to five mineral potential maps**

$Z_{AUC}$ is an *AUC* – dependent statistics satisfying standard normal distribution, it can be used to test whether the *AUC* value is significantly different from 0.5 with a probability of 95%. The five $Z_{AUC}$s in Table 6 are more than 1.96 of the 95% confidence limit, thus the five *AUC*s are significantly different from 0.5.

The *AUC*s and *AUL*s listed in Table 6 reveal that: (a) LGR performs best with *AUC* value 0.806 6 and *AUL* value 0.805 7; (b) *ASC* and *ASE* perform same nearly best with the identical *AUC* value 0.805 7 and the identical *AUL* value 0.804 8; (c) WofE performs well with *AUC* value 0.802 2 and *AUL* value 0.801 3; and (d) MLP performs worst with *AUC* value 0.658 0 and *AUL* value 0.657 5.

Based on the above discussion, performance of the five methods can be sequenced from the best to the worst as: LGR > *ASC* = *ASE* > WofE > MLP.

## 5 Discussion and conclusion

Cumulative gain and lift charts were introduced into the field of mineral prediction to evaluate the performance of mineral potential mapping models. A case study was conducted in the Altay region in northern Xinjiang in China. The WofE, LGR, RBM, and MLP models were applied to the mineral potential mapping and their performance were measured using their cumulative gain and lift charts. The results show that cumulative gain and lift charts are a feasible tool for estimating the effectiveness of mineral potential mapping models.

In our case study, the cumulative gain curves can differentiate the performance of WofE, LGR and MLP as well as the performance of RBM and MLP, but they can't differentiate the performance of RBM from that of WofE and LGR. The cumulative lift charts can differentiate the performance of RBM, WofE, and MLP and also the performance of LGR, WofE, and MLP, while can't discriminate the performance of RBM and LGR. Under those circumstances, the overall performance of the five methods were sequenced from the best to the worst using their *AUC* or *AUL* values.

The percentage of deposit-bearing cells is only 0.303 1% in the grid cell population in our case study. These class imbalance data make the values of *AUL* and *AUC* of each model almost identical and also make the cumulative gains and lift charts become polylines due to the situation that the number of deposit-bearing cells is far less than the number of thresholds.

The likelihood ratio is always non-negative. If the likelihood ratio is more than 1.0, the map pattern is positively associated with mineral deposits; and otherwise, the map pattern is negatively associated or unassociated with mineral deposits. So number 1.0 can serve as the fixed threshold value for map pattern selection. In practice, computing likelihood ratio is much simpler compared to computing the WofE contrast.

## References


Agterberg F P. 1974. Automatic contouring of geological maps to detect target areas for mineral exploration. *Mathematical Geology*, **6**(4): 373–395.

Agterberg F P. 1989. LOGDIA-FORTRAN 77 program for logistic regression with diagnostics. *Computers & Geosciences*, **15**(4): 599–614.

Agterberg F P. 1990. Combining indicator patterns for mineral resource evaluation//China University of Geosciences (eds.). Proceedings of International Workshop on Statistical Prediction of Mineral Resources. Wuhan: 1–15.

Agterberg F P. 1992. Combining indicator patterns in weights of evidence modeling for resource evaluation. *Nonrenewable Resources*, **1**(1): 39–50.

Agterberg F P, Bonham-Carter G F, Wright D F. 1990. Statistical pattern integration for mineral exploration//Gaal G, Merriam D F. (eds). Computer applications for mineral exploration in resource exploration. Oxford: Pergamon Press, 1–21.

Agterberg F P, Bonham-Carter G F. 1999. Logistic regression and weights of evidence modeling in mineral exploration//Proceedings of the 28th International Symposium on Applications of Computer in the Mineral Industry (APCOM), Golden, Colorado, 483–490.

Agterberg F P, Cheng Q M. 2002. Conditional independence test for weights-of-evidence modeling. *Natural Resources Research*, **11**(4): 249–255.

Anjum S. 2014. Composite indicators for data mining: A new framework for assessment of prediction classifiers. *Journal of Economics, Business and Management*, **2**(1): 62–67.

Bekkar M, Djemaa H K, Alitouche T A. 2013. Evaluation measures for models assessment over imbalanced data sets. *Journal of Information Engineering and Applications*, **3**(10): 27–38.

Bergmann R, Ludbrook J, Spooren W P J M. 2000. Different outcomes of the Wilcoxon-Mann-Whitney test from different statistics packages. *The American Statistician*, **54**(1): 72–77.

Berry M J A, Linoff G. 1999. Data mining techniques: for marketing, sales, and customer support. New York: John Wiley & Sons.

Bonham-Carter G F, Agterberg F P, Wright D F. 1988. Integration of geological datasets for gold exploration in Nova Scotia. *Photogrammetric Engineering and Remote Sensing*, **54**(11): 1585–1592.

Bonham-Carter G F, Agterberg F P, Wright D F. 1989. Weights-of-evidence modelling: a new approach to mapping mineral potential//Agterberg, F P, Bonham-Carter G F. (Eds.). Statistical applications in the earth sciences. Geological Survey of Canada, 171–183.

Burez J, Van den Poel D. 2009. Handling class imbalance in customer churn prediction. *Expert Systems with Applications*, **36**: 4626–4636.

Carranza E J M, Hale M. 2001. Logistic regression for geologically constrained mapping of gold potential, Baguio district, Philippines. *Exploration and Mining Geology*, **10**: 165–175.

Carranza E J M, Hale M. 2002a. Where are porphyry copper deposits spatially localized? A case study in Benguet province, Philippines. *Natural Resources Research*, **11**: 45–59.

Carranza E J M, Hale M. 2002b. Wildcat mapping of gold potential, Baguio district, Philippines. *Transactions Institute of Mining and Metallurgy (Applied Earth Science)*, **111**: 100–105.

Chen C H, Dai H Z, Liu Y, *et al.* 2011. Mineral prospectivity mapping integrating multisource geology spatial data sets and logistic regression modeling//Proceedings of IEEE International Conference on Spatial Data Mining and Geographical Knowledge Services (ICSDM), 214–217.

Chen Y L. 2015. Mineral potential mapping with a restricted Boltzmann machine. *Ore Geology Reviews*, **71**: 749–760.

Chen Y L, Lu L J, Li X B. 2014. Application of continuous restricted Boltzmann machine to identify multivariate geochemical anomaly. *Journal of Geochemical Exploration*, **140**: 56–63.

Flach P A, Hernandez-Orallo J, Ferri C. 2011. //Proceedings of the 28th International Conference on Machine

Learning (ICML-11), Bellevue, WA, USA, 657-664.

Japkowicz N. 2000. The class imbalance problem: Significance and strategies//Proceedings of the 2000 international conference on artificial intelligence (IC-AI'2000): Special track on inductive learning, Las Vegas, Nevada.

Li Z C. 1996. The evolution and formation of the left echelon volcanic-sedimentary basins in Altay and the tracing of their metallogenic activities. *Geotectonica et Metallogenia*, **20**(3): 189-200. (in Chinese with English Abstract)

Li Z C, Zhao Z H. 2002. Creation of the Altay orogenic belt and the Altay MTS. Tectono-metallogenic province. *Chinese Journal of Geology*, **37**(4): 483-490. (in Chinese with English Abstract)

Nykänen V, Groves D I, Ojala V J, *et al*. 2008. Combined conceptual/empirical prospectivity mapping for orogenic gold in the northern Fennoscandian Shield, Finland. *Australian Journal of Earth Sciences*, **55**(1): 39-59.

Piatetsky-Shapiro G, Steingold S. 2000. Measuring lift quality in database marketing. *ACM SIGKDD Explorations Newsletter*, **2**(2): 76-80.

Skabar A. 2007. Mineral potential mapping using Bayesian learning for multilayer perceptrons. *Mathematical Geology*, **39**(5): 439-451.

Tangestani M H, Moore F. 2001. Porphyry copper potential mapping using the weights-of-evidence model in a GIS, northern Shahr-e-Babak, Iran. *Australian Journal of Earth Sciences*, **48**(5): 913-927.

Tuffery S. 2005. Data mining et statistique decisionnelle. Paris: Edition TECHNIP.

Verbeke W, Martens D, Mues C, *et al*. 2011. Building comprehensible customer churn prediction models with advanced rule induction techniques. *Expert Systems with Applications*, **38**: 2354-2364.

Xie Y, Li X, Ngai E W T, *et al*. 2009. Customer churn prediction using improved balanced random forests. *Expert Systems with Applications*, **36**: 5445-5449.

Xu S, Cui Z K, Yang X L, *et al*. 1992. A preliminary application of weights of evidence in gold exploration in Xionger mountain region, Henan province. *Mathematical Geology*, **24**(6): 663-674.

Zeng Q S, Chen G H, Wang H, *et al*. 2005. Polygenetic compound metallogenic characteristics of the Ashele copper deposit in northern Xinjiang. *Geotectonica et Metallogenica*, **29**: 545-550. (in Chinese with English Abstract)